Supporting Information for

Differences of crystal structure and dynamics between soft porous nanocrystal and bulk crystal

Yuh Hijikata, Satoshi Horike, Daisuke Tanaka, Juergen Groll, Motohiro Mizuno, Jungeun Kim, Masaki Takata and Susumu Kitagawa

Department of Synthetic Chemistry and Biological Chemistry, Graduate School of Engineering, Kyoto University, Katsura, Nishikyo-ku, Kyoto 615-8510, Japan, DWI e.V. and Institute of Technical and Macromolecular Chemistry, RWTH Aachen University, Pauwelsstrasse 8, 52056 Aachen, Germany, Department of Chemistry, Graduate School of Natural Science & Technology, Kanazawa University, Kakuma-machi, Kanazawa 920-1192, Japan, Institute for Integrated Cell-Material Sciences (iCeMS), Kyoto University, Yoshida, Sakyo-ku, Kyoto 606-8501, Japan, ERATO Kitagawa Integrated Pores Project, Japan Science and Technology Agency (JST), Kyoto Research Park, Bulding#3, Shimogyo-ku, Kyoto, 600-8815, Japan, Japan Synchrotron Radiation Research Institute, 1-1-1, Kouto, Sayo-cho, Sayo-gun, Hyogo 679-5198, Japan, and RIKEN, SPring-8 Center, 1-1-1, Kouto, Sayo-cho, Sayo-gun, Hyogo 679-5148, Japan

Physical Measurements

Thermogravimetric analyses (TGA) were performed using a Rigaku Thermo plus TG 8120 apparatus with a temperature range between 298 and 773 K in an atmosphere of N_2 and at a heating rate of 10 K.min^{-1}. X-ray powder diffraction (XRPD) data were collected at 298 K using a Rigaku RINT-2200HF (Ultima) diffractometer with CuKα radiation. Solid-state ^{2}H NMR spectra were measured at 298 K on a Varian Chemagnetics CMX-300 spectrometer operated at 45.826 MHz by using a quadrupole echo pulse sequence. Hitachi S-4800 field-emission scanning electron microscopy (FE-SEM) was used to obtain the morphology and size distribution of NCID-1. The infrared spectra were measured using KBr disks employing a Perkin-Elmer Spectrum BX FT-IR

Syntheses

Synthesis of {[$Zn_2(ip)_2(bpy)_2$]·DMF}$_n$ and [Zn(ip)(bpy)]$_n$ (CID-1⊃DMF and CID-1)

All reagents were obtained from commercial suppliers and used without further purification. {[$Zn_2(ip)_2(bpy)_2$]·DMF}$_n$ (CID-1⊃DMF) and [Zn(ip)(bpy)]$_n$ (CID-1) were prepared according to methods previously reported.[1] Briefly, isophthalic acid (H_2ip) (0.85 mmol, 141 mg), 4,4′-bipyridyl (bpy) (0.85 mmol, 133 mg), and $Zn(NO_3)_2·6H_2O$ (0.85 mmol, 253 mg) were dissolved in 50 ml of *N*,*N*-dimethylformamide (DMF). The solution was stirred at 120 °C for 2 days. After cooling, the resulting white precipitate was isolated by filtration and washed with fresh DMF. The obtained powder was CID-1⊃DMF. CID-1 was obtained after drying at 150 °C for 12 hours under vacuum. The CID-1⊃DMF powder diffraction data are shown in Figures S1.

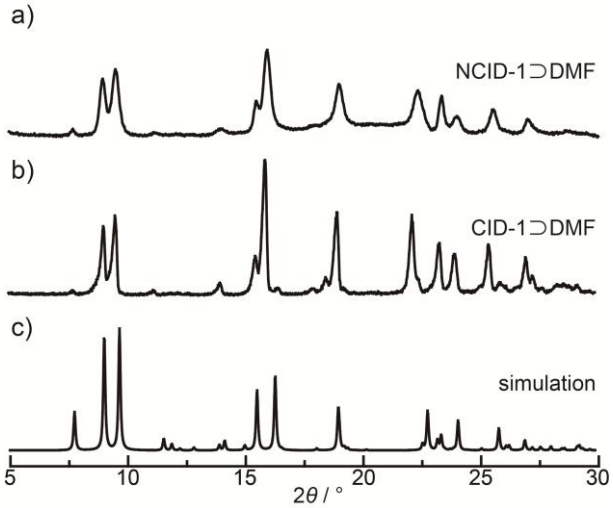

Figure S1. XRPD of (a) NCID-1⊃DMF and (b) CID-1⊃DMF, and (c) the simulated CID-1⊃DMF pattern produced using X-ray diffraction data from a single crystal.

Synthesis of a Single Crystal of CID-1

An as-synthesized single crystal of CID-1⊃DMF was soaked in methanol for a week. The single crystal was heated at 150 °C under a stream of N_2 for 6 hours and dried at 150 °C for 12 hours under vacuum. Single-crystal X-ray diffraction data was collected at 223 K using a Rigaku/MSC Saturn CCD diffractometer with confocal monochromated MoKα radiation (λ = 0.7107 Å) and processed using CrystalClear software (Rigaku). The crystal structure was solved using a direct method (Sir 97) and refined by a full matrix least-squares method using SHELXL-97 software. The position of nonhydrogen atoms was refined with anisotropic displacement factors. The position of hydrogen atoms was identified and refined using a riding model. These data can be obtained free of charge from the Cambridge Crystallographic Data Centre via www.ccdc.cam.ac.uk/data_request/cif.

Synthesis of bpy-d_8

Bpy-d_8 was synthesized using the followed procedure.[2] In a Teflon vessel, D_2O (15 mL) was added to Pt_2O (0.1 mmol, 22.7 mg) and bpy (2.0 mmol, 310 mg) after grinding. After the vessel was sealed, it was heated at 250 °C for 8 hours. After cooling, the obtained mixture was extracted with $CHCl_3$, and $CHCl_3$ solution was dried Na_2SO_4. The pale-yellow powder obtained after evaporation was recrystallized from CH_3OH with H_2O. Deuteration was characterized by NMR and MS.

Synthesis of CID-1-*d*

CID-1-*d* was synthesized with bpy-d_8 using the same procedure as described for nondeuterated CID-1. The CID-1-*d* powder diffraction data are shown in Figure S2.

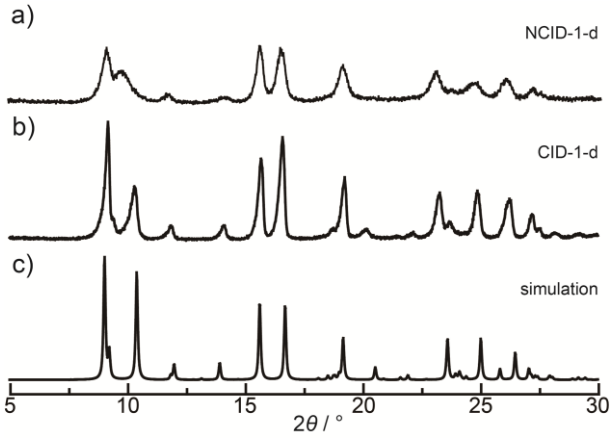

Figure S2. XRPD of (a) NCID-1-*d* and (b) CID-1-*d*, and (c) the simulated CID-1 pattern produced using X-ray diffraction data from a single crystal.

Synthesis of CID-1 Nanoparticles (NCID-1)

NCID-1 was prepared according to a previous report.[3] H_2ip, bpy, and $Zn(NO_3)_2 \cdot 6H_2O$ were dissolved in DMF (192 ml). The concentration of each of the three components was 100 mM. After maintaining this solution at ambient temperature for 10 min, 5 ml of AOT/*n*-heptane solution (500 mM) was injected into it, and it was sonicated for 10 min. The obtained nanoparticles were collected by centrifugation. The particles were washed by sonication in ethanol. After drying the precipitate under reduced pressure at 150 °C for 24 h, we obtained NCID-1. The size distribution is similar to the value reported in previous work, which are around 324±100 nm in length and 50±15 nm in width.[3] The morphology of NCID-1 is shown in FE-SEM image (Figure S3). IR spectrum of NCID-1 are shown in Figure 4S. IR spectrum of NCID-1 has the broad peaks around 1713 cm-1 comparing with CID-1, which suggest the ester group of AOT coordinating to Zn ions. In Figure S6 and S7, the first large loss of 40.8% for CID-1 and 38.2% for NCID-1 indicate the loss of bpy. The calculated amount of AOT is 0.070 molecules per one Zn ion based on these value.

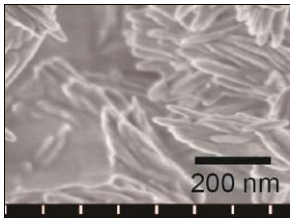

Figure S3. The FE-SEM image of NCID-1 particles.

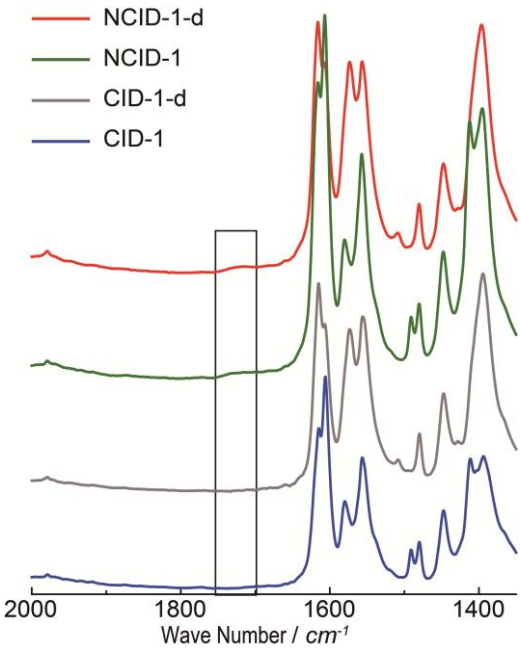

Figure S4. IR spectra of CID-1 (blue line), CID-1-d (gray line), NCID-1 (green line), NCID-1-d (red line)

Synthesis of CID-1-*d* Nanoparticles (NCID-1-*d*)

NCID-1-*d* was synthesized using bpy-d_8 using the same procedure as described for nondeuterated NCID-1. The NCID-1-*d* powder diffraction data and IR spectrum are shown in Figure S2 and S4, respectively.

Removal of Guest Molecules

CID framework releases DMF molecules around 150 °C with clear decrease. The amount of DMF decreasing is corresponding to one DMF molecule per one pore, as shown in Figure S5. After evacuation at 150 °C, guest DMF molecules were removed, shown in Figure S6 and S7. CID-1, CID-1-*d*, NCID-1, and NCID-1-I have no DMF molecule in their pores based on TGA curves.

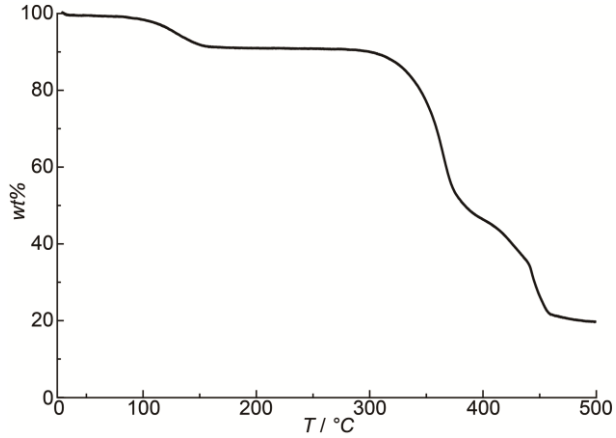

Figure S5. TGA curves of CID-1⊃DMF over the temperature range from 25-500 °C at a heating rate of 10 °C min^{-1} under the N_2 atmosphere

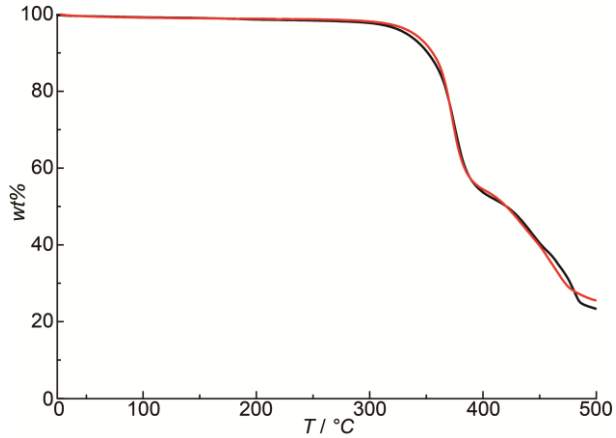

Figure S6. TGA curves of CID-1 (black line) and CID-1-*d* (red line) over the temperature range from 25-500 °C at a heating rate of 10 °C min^{-1} under the N_2 atmosphere

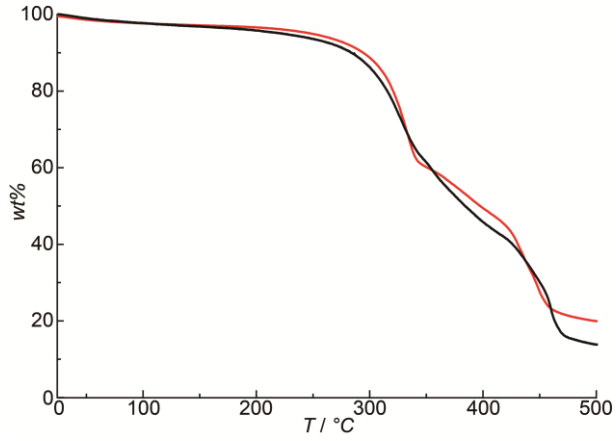

Figure S7. TGA curves of NCID-1 (black line) and NCID-1-*d* (red line) over the temperature range from 25-500 °C at a heating rate of 10 °C min^{-1} under the N_2 atmosphere

Synchrotron Powder X-ray Diffraction Measurement and Analysis

The powder samples of NCID-1 and NCID-1⊃DMF were sealed in a silica glass capillary. XRPD patterns with good counting statistics were measured at 298 K for 1 hour using a synchrotron radiation XRPD experiment with a large Debye–Scherrer camera, and imaging plates as detectors on the BL02B2 beam line at the Super Photon Ring (SPring-8). The radiation wavelength was 0.99824 Å for NCID-1 and 0.80006 Å for NCID-1⊃DMF. The cell parameters determined by single-crystal X-ray analysis of CID-1 and CID-1⊃DMF were applied as the initial unit cell parameters. Refinements of unit cell parameters for NCID-1 and NCID-1⊃DMF were conducted using the Le Bail fitting method. The unit cell parameters are shown in Tables S1 and S2. The obtained diffraction patterns are shown in Figures S8 and S9, respectively. The cell parameters of CID-1⊃DMF at 223 K and NCID-1⊃DMF at 298 K are quite similar, on the other hand the cell parameters of CID-1 and NCID-1 are clearly different.

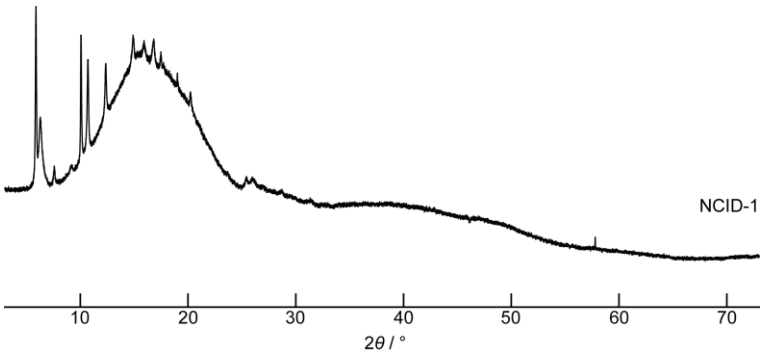

Figure S8. NCID-1 synchrotron XRPD pattern. The wavelength was 0.99824 Å.

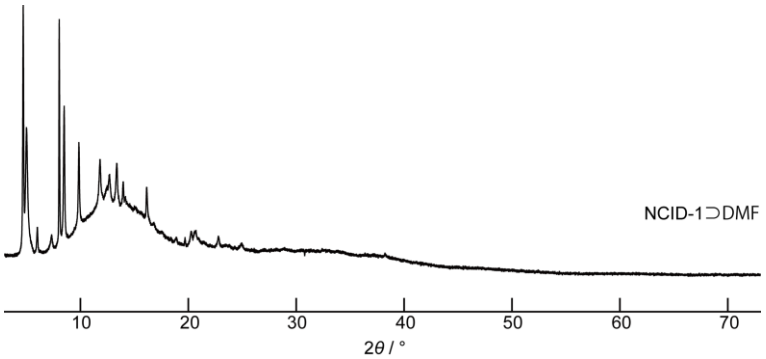

Figure S9. NCID-1⊃DMF synchrotron XRPD pattern. The wavelength was 0.80006 Å.

Table S1. **Cell parameters of CID-1 and NCID-1**

	a (Å)	*b* (Å)	*c* (Å)	*α* (°)	*β* (°)	*γ* (°)
CID-1	8.9568 (18)	10.087 (2)	10.1225 (19)	78.209 (9)	73.265 (8)	79.154 (9)
NCID	9.55936 (221)	10.03497 (124)	9.71231 (464)	77.94537 (1908)	72.32541 (2272)	79.01543 (4144)

Table S2. **Cell parameters of CID-1⊃DMF and NCID-1⊃DMF**

	a (Å)	*b* (Å)	*c* (Å)	*α* (°)	*β* (°)	*γ* (°)
CID-1⊃DMF	10.082 (5)	11.384 (5)	15.744 (8)	90	103.917 (8)	90
NCID⊃DMF	10.08656 (217)	11.40997 (132)	15.74710 (342)	90	104.19211 (1332)	90

Details for Simulations of Solid-state ^{2}H NMR Spectra

To reveal the line shape of ^{2}H NMR spectra, spectral simulations were performed using custom written FORTRAN programs. Mobility of ^{2}H atoms in bpy-d_8 of CID-1 and NCID-1 was observed. The mobility is rotational or flip around the N–N axis, which is the C_2 axis of bpy bonding to the Zn atoms, as shown in Figure S10 and S11. Both CID-1 and CID-1⊃guest have a 0D pore surrounded by bpy, and therefore the guest adsorption process would be affected by the mobility of bpy that we investigated. The mobility of two pyridyl rings in CID-1 was simulated as a 2-site jump along the C_2 axis based on the single-crystal structure of CID-1 with a quadrupole coupling constant (e^2Qq/h : QCC), 172 kHz. The simulated spectrum showed agreement with the experimental spectrum. The bpy in CID-1 has two crystallographically independent pyridyl rings, and one pyridyl ring is sterically restrained by the isophthalate of the neighbor layer in its mutually interdigitated structure. The frequencies of mobility of the two pyridyl rings are k = 4 MHz and less than k = 1 kHz, which is the lower limitation for observing the dynamics for ^{2}H NMR. The simulated spectrum is the summation of simulated spectra for the lower (k = 0 kHz) and higher (k = 4.0 MHz) mobility of the pyridyl ring. A similar model of simulation was applied to NCID-1, and the simulated spectrum is the summation of simulated spectra of lower (k = 8.0 kHz) and higher (k = 100 MHz) mobility of the pyridyl ring. Because the observable range of frequency for ^{2}H NMR is from 10^3 to 10^7, we can estimate that the highest mobility of the pyridyl ring in NICD-1 is over 10 MHz. This increase in mobility is caused by the sliding of layers as described in the main manuscript. Both spectra of CID-1 and NCID-1 have extra peaks around ±10 kHz that are not able to be predicted based on the single-crystal structure of CID-1. Although we have not produced a simulation to reproduce and analyze the extra peaks, we can confidently mention that an increase of mobility occurred in NCID-1 compared with that in CID-1.

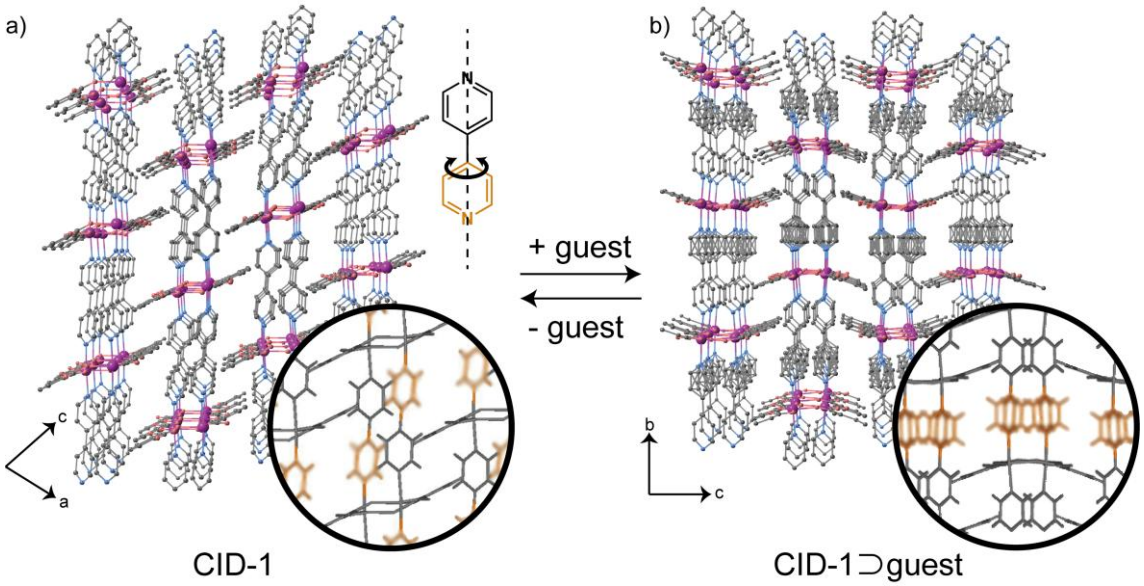

Figure S10. The assembled structures of (a) CID-1 and (b) CID-1⊃DMF (without DMF). The hydrogen atoms are omitted for clarity. CID-1 and CID-1⊃DMF have pyridyl rings sterically restrained by adjacent isophthalates, and sterically free pyridyl rings. In the illustrations of the expanded structure (in circles) showing hydrogen atoms, the gray pyridyl rings with restraint by isophthalates have a lower mobility than the orange pyridyl rings.

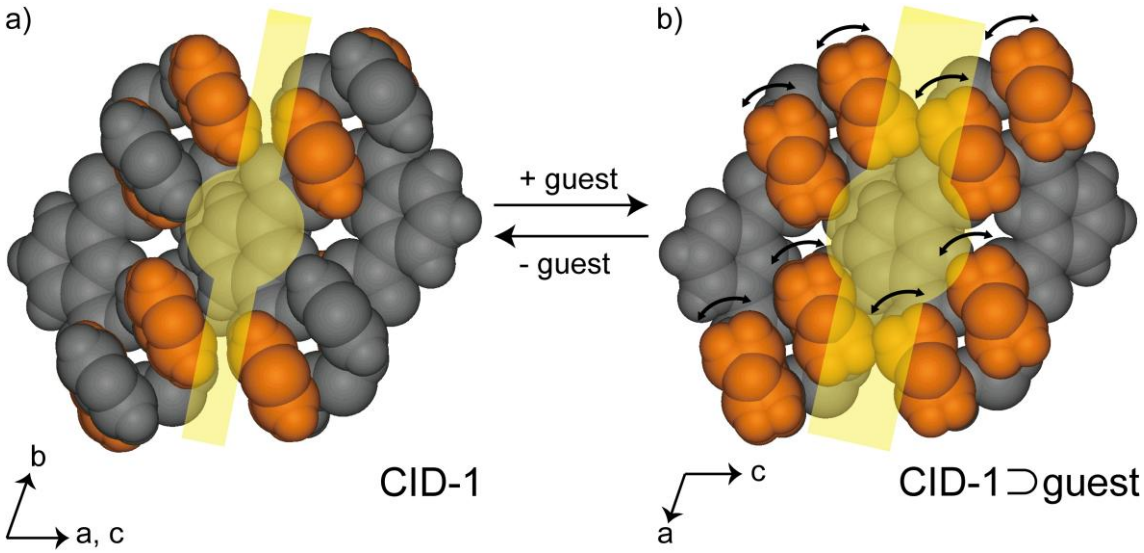

Figure S11. The pore structure of (a) CID-1 and (b) CID-1⊃DMF. Guest DMF are omitted. Black arc arrows are ranges of the dynamic disordering of bpy moieties. Orange parts are pyridyl rings with high mobility, and the yellow shapes show 0D cavity and diffusion path.

Reference

(1) Horike, S.; Tanaka, D.; Nakagawa, K.; Kitagawa, S. *Chem. Commun.* **2007**, 3395.

(2) Yamamoto, M.; Oshima, K.; Matsubara, S. *Heterocycles* **2006**, *67*, 353.

(3) Tanaka, D.; Henke, A.; Albrecht, K.; Moeller, M.; Nakagawa, K.; Kitagawa, S.; Groll, J. *Nat. Chem.* **2010**, *2*, 410.